



Article

Ethanol-Quenching Introduced Oxygen Vacancies in Strontium Titanate Surface and the Enhanced Photocatalytic Activity

Yang Xiao ¹, Shihao Chen ¹, Yin Hai Wang ^{1,*} , Zhengfa Hu ², Hui Zhao ¹ and Wei Xie ³

¹ School of Physics & Optoelectronic Engineering, Guangdong University of Technology, Guangzhou 510006, China; xiaognay@163.com (Y.X.); shchenbhx@163.com (S.C.); kkhui@gdut.edu.cn (H.Z.)

² Synergy Innovation Institute for Modern Industries, Guangdong University of Technology, Dongyuan 517500, China; zhfh@gdut.edu.cn

³ School of Physics Science and Technology, Lingnan Normal University, Zhanjiang 524048, China; xiwei@lingnan.edu.cn

* Correspondence: yhwang@gdut.edu.cn; Tel.: +86-020-39322265

Received: 23 May 2019; Accepted: 10 June 2019; Published: 14 June 2019



Abstract: Modification of the surface properties of SrTiO₃ crystals by regulating the reaction environment in order to improve the photocatalytic activity has been widely studied. However, the development of a facile, effective, and universal method to improve the photocatalytic activity of these crystals remains an enormous challenge. We have developed a simple method to modify the surface environment of SrTiO₃ by ethanol quenching, which results in enhanced UV, visible and infrared light absorption and photocatalytic performance. The SrTiO₃ nanocrystals were preheated to 800 °C and immediately quenched by submersion in ethanol. X-ray diffraction patterns, electron paramagnetic resonance spectra, and X-ray photoelectron spectra indicated that upon rapid ethanol quenching, the interaction between hot SrTiO₃ and ethanol led to the introduction of a high concentration of oxygen vacancies on the surface of the SrTiO₃ lattice. Consequently, to maintain the regional charge balance of SrTiO₃, Sr²⁺ could be substituted for Ti⁴⁺. Moreover, oxygen vacancies induced localized states into the band gap of the modified SrTiO₃ and acted as photoinduced charge traps, thus promoting the photocatalytic activity. The improved photocatalytic performance of the modified SrTiO₃ was demonstrated by using it for the decomposition of rhodamine B and production of H₂ from water under visible or solar light.

Keywords: photocatalysis; SrTiO₃; ethanol-quenching; oxygen vacancies; photodegradation; photocatalytic H₂ generation

1. Introduction

Since the discovery of photoelectrochemical water splitting on a titania electrode by Fujishima and Honda in 1972, photocatalysis using semiconductors has been widely studied [1]. Semiconductor-based photocatalysts are capable of directly converting solar energy to chemical energy, which provides a facile approach for environmental protection and H₂ production under sunlight irradiation [2–4]. Among these semiconductors, titanium dioxide (TiO₂) has attracted special interest because of its chemical stability, non-toxicity, and low cost [5,6]. In addition, Strontium titanate (SrTiO₃), a perovskite-type oxide, has been classified a wide-band gap (3.1–3.7 eV) semiconductor photocatalyst in the field of light energy exploitation. SrTiO₃ possesses various outstanding physical and chemical properties such as good chemical/catalytic stability, suitable band position, and susceptibility to change by other substance. Notably, the conduction band of SrTiO₃ is more negative than that of TiO₂, which is

beneficial for photocatalysis [7]. However, because of its large band-gap, SrTiO₃ can be utilized only in the UV region of sunlight, which largely restricts its practical application in photocatalysis [8,9].

Many studies have attempted to expand the spectral response of SrTiO₃ by utilizing methods such as doping with a metal/nonmetal, or co-doping with a nonmetal to form a new intermediate gap state between the valence band (VB) and the conduction band (CB) [10–14]. Moreover, mixing of the energy levels of the dopant and host elements can change the position of the VB or CB, resulting in increased visible light absorption [9]. However, the rapid rate of recombination of the electron-hole pairs in SrTiO₃ results in poor photocatalytic efficiency. One of the methods to improve the separation efficiency of photogenerated electron-hole pairs involves combination with other noble metals (usually Pt, Au, and Rh) or semiconductors on the surface [15–18]. In the other hand, the important role played by surface oxygen vacancies in improving the photocatalytic performance is well known. Surface oxygen vacancies can be used as surface adsorption sites and photoinduced charge traps, where the charge shifts to the adsorbed compound, so that the recombination of photogenerated electron-holes is prevented and the photocatalytic performance is improved [19,20]. Therefore, introducing oxygen vacancies on the surface of the SrTiO₃ lattice seems to be a feasible process to modify the surface environment of SrTiO₃. This process could improve the adsorption capacity of SrTiO₃ and inhibit the recombination of photogenerated electron-hole pairs, thus improving the photocatalytic performance of SrTiO₃ [21].

In 2011, Mao and co-worker developed black TiO₂ by introducing disorder in the surface layer of TiO₂ via hydrogenation in a high H₂-pressure atmosphere at about 200 °C for 5 days. This modification greatly enhanced the solar light harvesting efficiency and photocatalytic activity of TiO₂ [22]. Subsequently, various methods were developed to synthesize hydrogenated or reduced semiconductors such as TiO₂, ZnO and WO₃ with surface oxygen defects for improving their photocatalytic performance [23–26]. Unsurprisingly, hydrogenated or reduced SrTiO₃ was also synthesized. Tan et al. introduced oxygen vacancies on the SrTiO₃ surface by heating it to 300–375 °C under Ar atmosphere, to control any solid-state reaction between NaBH₄ and SrTiO₃, which improved its photocatalytic activity for H₂ generation under UV-vis irradiation [19]. Zhao et al. prepared black SrTiO₃ with abundant Ti³⁺ cations and oxygen vacancies by reduction using molten aluminum at 500 °C. The black SrTiO₃ showed enhanced light absorption in the visible and near-infrared region and remarkable photocatalytic performance [27]. However, some questions regarding the photocatalytic practical applications of SrTiO₃ remain unanswered. The preparation conditions of these modified SrTiO₃ photocatalyst are too complex, hazardous, and costly, thus hindering the extensive application of this compound in photocatalysis.

Supphasrironjaroen et al. demonstrated that rapid quenching in different media can lead to the formation of Ti³⁺ self-dopants in TiO₂, thus improving the photocatalytic activity of TiO₂-based materials [28]. Herein, we report a facile method to prepare SrTiO₃ rich in oxygen vacancies, with improved photocatalytic performance in the visible region. SrTiO₃ was preheated to a high temperature, followed by rapid submersion in ethanol, resulting in the darkening of the color of SrTiO₃. Various structural and electronic analyses revealed the introduction of oxygen vacancies in the quenched SrTiO₃ (Q-SrTiO₃), resulting in increased photocatalytic activity. The photocatalytic performance of Q-SrTiO₃ was evaluated by using it for the degradation of rhodamine B (RhB) dye and the photolysis of water to produce H₂, with the original SrTiO₃ as a control. The results indicated the enhanced photocatalytic activity of Q-SrTiO₃.

2. Materials and Methods

2.1. Preparation of Q-SrTiO₃

1 g of original SrTiO₃ nanoparticles (99.5%, ~100 nm, Macklin Biochemical, Germany) was weighed using an electronic scale, then 1 g of original SrTiO₃ was put in a sintering boat (length 6 cm, width 3 cm, height 1.5 cm). When the Muffle furnace heat to 800 °C, the sintering boat along with

1 g of original SrTiO₃ was transferred to the Muffle furnace. The SrTiO₃ nanoparticles were heated at 800 °C for 20 min, and then open the Muffle furnace door, immediately took out the sintering boat and submerged the SrTiO₃ in 45 mL ethanol (AR) at room temperature for rapid quenching. Afterwards, the quenched sample was filtered and then dried at 80 °C for 3 h for further use.

2.2. Characterization

An X-ray diffractometer (XRD, D8 ADVANCE, Bruker, Karlsruhe, Germany) was used to check the phase structures of all the samples. Data were collected between 20° and 80° (2θ) with a 0.02° step size using Cu Kα irradiation, at 36 kV tube voltage and 20 mA tube current. Field-emission transmission electron microscopy (FE-TEM, Talos F200S, FEI, Thermo, Hillsboro, OR, USA) and Field-emission scanning electron microscopy (FE-SEM, SU8220, Hitach, Tokyo, Japan) was used to determine the surface change, particle size and morphology of the samples. Sample specimens for the FE-TEM and the FE-SEM observations were prepared as follows: The powdered sample was dispersed in ethanol in an ultrasonic washing bath, and then, a drop of the suspension was dripped slightly onto a micro grid or a silicon slice and dried before imaging. X-ray Photoelectron Spectroscopy (XPS, Escalab 250Xi, Thermo Fisher, Bremen, Germany) was used to analyze the chemical composition and relative amount of the elements on the surface of the samples, with a reference of C1 s and the excitation source of 150 W Al Kα X-rays. An Electron paramagnetic resonance spectrometer (EPR, EMXplus-10/12, Bruker, Karlsruhe, Germany) was used to detect unpaired electrons in the samples at room temperature. A UV-Vis-NIR spectrophotometer (DRUV-vis, UV-3600 Plus, SHIMADZU, Kyoto, Japan) were used to record the UV-vis diffuse reflectance absorption in the range of 200–2000 nm.

2.3. Photocatalytic Test

2.3.1. Photocatalytic Degradation of RhB

The photocatalytic degradation activities of Q-SrTiO₃ were evaluated by monitoring the rate of decomposition of RhB in an aqueous solution under visible-light or UV-light irradiation from a 500 W Xe lamp equipped with a UV cut off filter (>420 nm) or 500 W Hg lamp, the light intensity of 500 W Xe lamp equipped with a UV cut off filter and 500 W Hg lamp are 6 mW/cm² and 48 mW/cm², respectively. A cylindrical Pyrex vessel equipped with a lamp was used as the photocatalytic reactor, with water circulation to keep the reaction temperature at about 27 °C. 40 mL of an aqueous solution of RhB (4 × 10⁻⁵ M) and 0.02 g Q-SrTiO₃ or SrTiO₃ were placed in a quartz tube for the degradation reaction. Before the photodegradation, a dark reaction was conducted for 30 min to ensure adsorption-desorption equilibrium between the photocatalyst and the RhB solution. Continuous magnetic stirring was carried out to keep the photocatalyst suspended in the RhB solution. Next, the mixture was exposed to visible light or UV light. The samples were collected at regular intervals (1.5 h or 1 h), and the concentration of RhB in the solution was determined using a UV-Vis spectrophotometer at 553 nm. The percentage of degradation was recorded as C/C_0 , and the reaction constant (K_{app}) was calculated from the slope of the linear regression obtained from the plot of $-\ln(C/C_0)$ vs. time, where C_0 and C are the absorbance of the RhB solution initially and at a particular time, respectively.

2.3.2. Photocatalytic Evolution of hydrogen

The photocatalytic H₂ production experiments were conducted in a 400 mL Pyrex quartz glass reactor at normal pressure and temperature. The photocatalyst (100 mg) was dispersed in 100 mL of 10% aqueous methanol solution (methanol acting as a sacrificial agent) using a magnetic stirrer. Then the reaction mixture was dispersed in an ultrasonic washing bath for 10 min. Before the irradiation by a 300 W Xe lamp (CRL-HXF300, China) as the sunlight source, the reactor was deaerated with nitrogen gas. During the photocatalytic reaction, the reactant solution was maintained at room temperature by using a Low-temperature cooling circulating pump (CEL-CR300, China), and magnetic stirring was continually maintained to keep the photocatalyst suspended in the aqueous methanol solution.

The amount of H₂ generated was tested using an online Shimadzu GC-2014C gas chromatograph (Shimadzu, Japan) equipped with an MS-5A column. The total reaction time for each sample was 5 h, and the H₂ concentration was measured every hour.

3. Results and Discussion

3.1. Characterization of the Photocatalysts

The peaks in the powder XRD patterns of SrTiO₃ and Q-SrTiO₃ (Figure 1) matched with the (100), (110), (111), (200), (210), (211), (220) and (310) planes, indicating a characteristic SrTiO₃ cubic structure (JCPDS card: 73-6001). Moreover, a small peak for SrCO₃ was observed, probably due to the coexistence of SrTiO₃ and SrCO₃ under the atmospheric operating conditions adopted in the hydrothermal method [29]. No other diffraction peak was observed in the XRD patterns. Comparison with the XRD patterns from the local enlargement of the diffraction peaks (inset of Figure 1) revealed a slight shift ($2\theta \sim 0.15^\circ$) of the (110) peak to a lower angle for Q-SrTiO₃. According to the Bragg equation ($2d \sin \theta = \lambda$, where d , θ and λ are the crystal spacing, diffraction angle, and X-ray wavelength, respectively), a shift in the diffraction peaks toward a lower angle suggests an increase in the lattice parameters. This might be attributed to the substitution of Sr²⁺ (ionic radius Sr²⁺ > Ti⁴⁺) for Ti⁴⁺ in Q-SrTiO₃ [30].

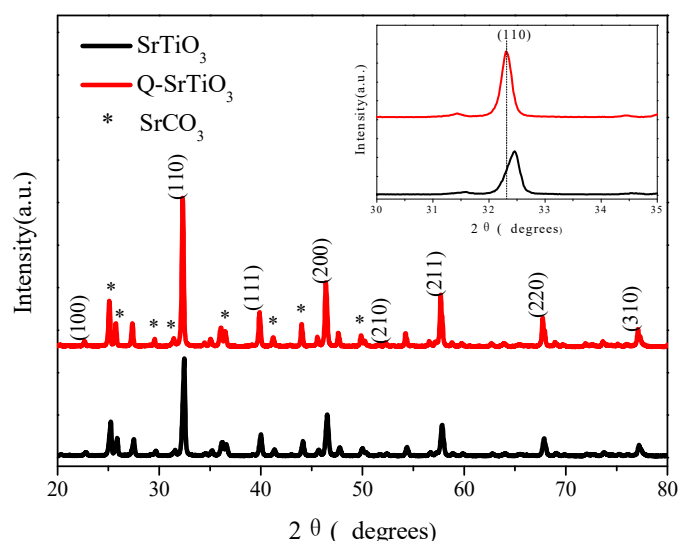


Figure 1. XRD patterns of SrTiO₃ and Q-SrTiO₃ samples.

The UV-visible absorption spectra of SrTiO₃ and Q-SrTiO₃ (Figure 2a) exhibited an absorption onset at ~400 nm, which corresponds to a band gap of 3.1 eV. In contrast to the SrTiO₃, the photoabsorption of Q-SrTiO₃ was dramatically enhanced in the both UV, visible and infrared light regions, consistent with the color change of the sample from white to gray (inset of Figure 2a). The improved light absorption was attributed to the formation of surface oxygen vacancies in Q-SrTiO₃. Similar results have been observed in other studies [19,31].

EPR is highly sensitive to unpaired electrons; hence, it was used for the detection of oxygen vacancies and Ti³⁺ species in SrTiO₃ and Q-SrTiO₃ (Figure 2b). Both SrTiO₃ and Q-SrTiO₃ showed a distinct EPR signal at $g = 1.977$ and $g = 2.002$, which could be ascribed to Ti³⁺ and oxygen vacancies, respectively. Because of its intrinsic non-stoichiometry, SrTiO₃ always contains a fraction of oxygen vacancies and Ti³⁺ ions [32]. EPR spectra revealed that Q-SrTiO₃ exhibited a stronger signal intensity for oxygen vacancies than did SrTiO₃, indicating the presence of more oxygen vacancies in Q-SrTiO₃, thus favoring enhanced photocatalytic activity of the Q-SrTiO₃. Takata and Domen also demonstrated that doping of a cation with a lower valence ion than that of the parent cation (such as Sr²⁺ in SrTiO₃) can introduce oxygen vacancies, thus effectively improving its photocatalytic activity [32]. Thus, based on

the XRD results, due to the exists of abundant oxygen vacancies, in order to keep the regional charge balance of the Q-SrTiO₃, the Sr²⁺ ions could substituted for Ti⁴⁺ ions, so that lattice expansion occurs (Figure 2c) [32,33].

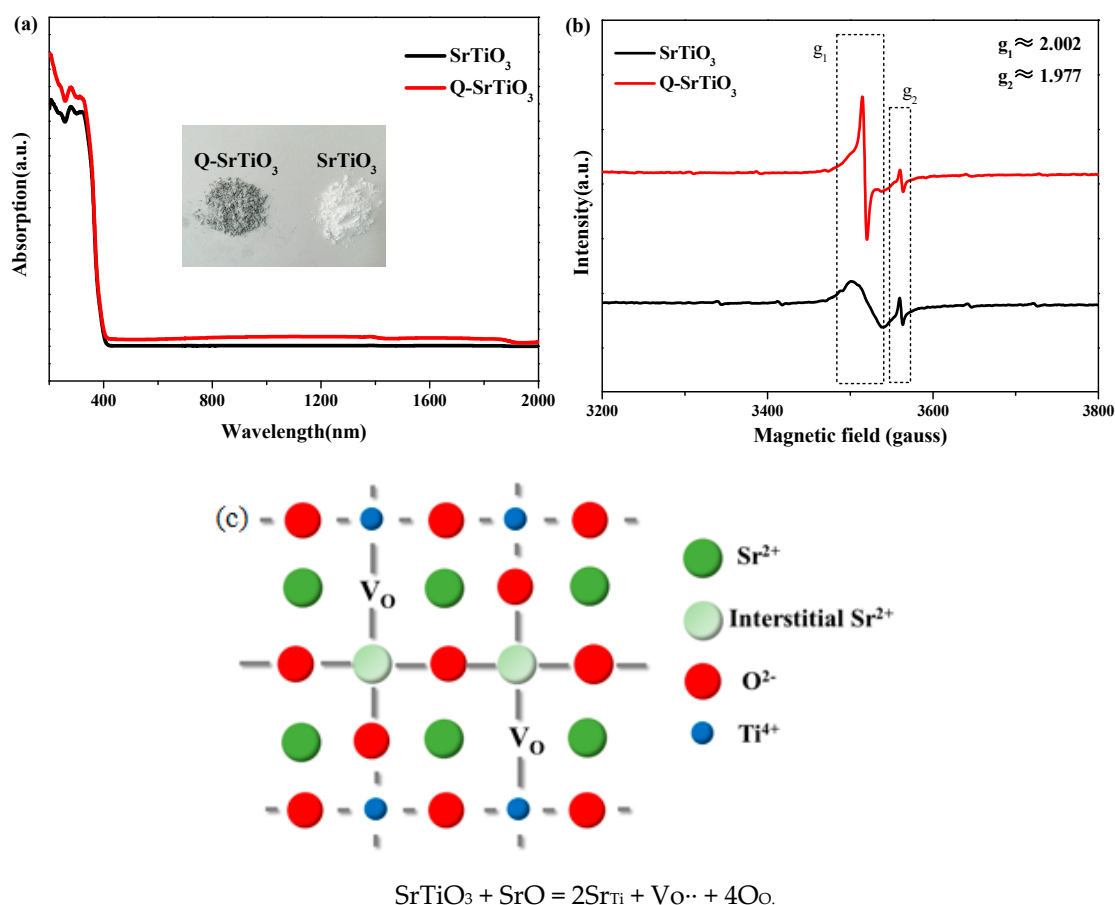


Figure 2. UV-vis absorption spectra of SrTiO₃ and Q-SrTiO₃ (a), the insert is a photograph of SrTiO₃ and Q-SrTiO₃; EPR spectra of SrTiO₃ and Q-SrTiO₃ (b). Schematic illustration of lattice change of Q-SrTiO₃ after solvent-quenching (c).

The high-resolution transmission electron microscopy (HR-TEM) images (Figure 3a,b) revealed the interplanar spacing of SrTiO₃ and Q-SrTiO₃ crystals to be ~0.27 nm, which is consistent with the d-spacings of the (110) crystallographic planes of cubic SrTiO₃. However, Liu et al. have reported that an ice-water quenching TiO₂ had introduced a disordered surface layer surrounding the crystalline core, and the surface lattice distortion is related to the generation of oxygen vacancies during the ice-water quenching [34]. In contrast, Q-SrTiO₃ prepared in this work used 800 °C ethanol quenching that did not lead to specific disordered surface layer, therefore, the generation of more oxygen vacancies in Q-SrTiO₃ have not introduced disordered surface layer. The SEM images (Figure 3c,d) revealed the particle size and particle morphology of Q-SrTiO₃ and SrTiO₃ show no change, and the average diameters of Q-SrTiO₃ and SrTiO₃ nanocrystals are ~100 nm, hence, ethanol-quenching can not change the particle size and particle morphology of samples.

XPS was used to investigate the surface chemical composition and VB position of SrTiO₃ and Q-SrTiO₃. The Sr 3d_{5/2}, Sr 3d_{3/2}, Ti 2p_{1/2}, and Ti 2p_{3/2} binding energies were 133.2, 134.6, 458.0, and 464.0 eV, respectively, in accordance with the literature values (Figure 4a,b) [35]. The Sr 3d and Ti 2p spectra showed no obvious variation between SrTiO₃ and Q-SrTiO₃. The Sr/Ti ratio of the samples was estimated according to the peak area and sensitivity factor of Sr 3d and Ti 2p (Table 1). The atomic ratio of Sr to Ti on the surface was about 1.64 and 2.15 for SrTiO₃ and Q-SrTiO₃, respectively. The larger

atomic ratio of Sr/Ti in Q-SrTiO₃ than that in SrTiO₃ might be due to the substitution of Sr²⁺ for Ti⁴⁺ on the surface of the former.

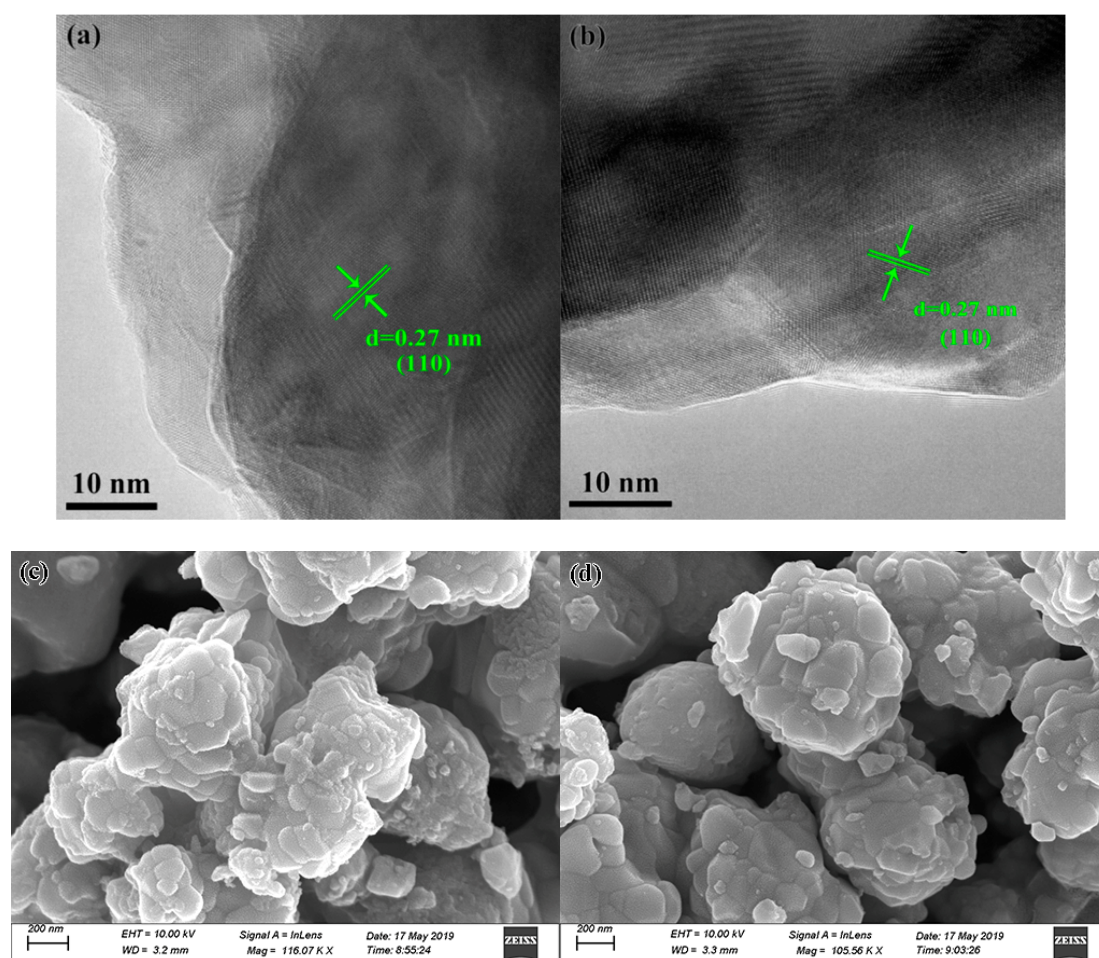


Figure 3. High-resolution TEM images and SEM images of SrTiO₃ (a,c) and Q-SrTiO₃ (b,d).

Table 1. Summary of the XPS data for the SrTiO₃ and Q-SrTiO₃.

Sample	Atomic Concentration (%)				Atomic Ratio
	Ti	Sr	O	C	Sr/Ti
SrTiO ₃	3.73	6.14	31.36	58.76	1.64
Q-SrTiO ₃	2.83	6.10	29.75	61.32	2.15

The O 1s high-resolution X-ray photoelectron spectra of SrTiO₃ and Q-SrTiO₃ showed two typical components of SrTiO₃ (Figure 4c). The two peaks located at 529.2 and 531.5 eV were assigned to bulk oxygen and surface oxygen in the samples, respectively. Based on previous research, it was assumed that the peak intensity of surface oxygen was related to the concentration of oxygen vacancies on the surface of SrTiO₃ and Q-SrTiO₃ [19,36]. The peak intensity at 531.5 eV become stronger for Q-SrTiO₃, indicating that the concentration of oxygen vacancies on the surface of Q-SrTiO₃ increased after the ethanol-quenching process. The introduction of more oxygen vacancies on the surface of Q-SrTiO₃ lattice resulted in impure/defect states in the band gap, enhancing the visible and near infrared-light absorption of Q-SrTiO₃ [27]. Furthermore, the increased amount of oxygen vacancies can improve the efficient charge transport in Q-SrTiO₃, followed by the Fermi level shift toward to the CB of the Q-SrTiO₃, facilitating the separation of photogenerated electron-hole pairs and resulting in enhanced photocatalytic activity [19,27]. In the VB XPS profile, the VB maxima were estimated by

linear extrapolation of the peaks to the baselines (Figure 4d). Both, SrTiO₃ and Q-SrTiO₃ displayed identical VB band positions at 2.3 eV below the Fermi energy, indicating no shift in the VB edge.

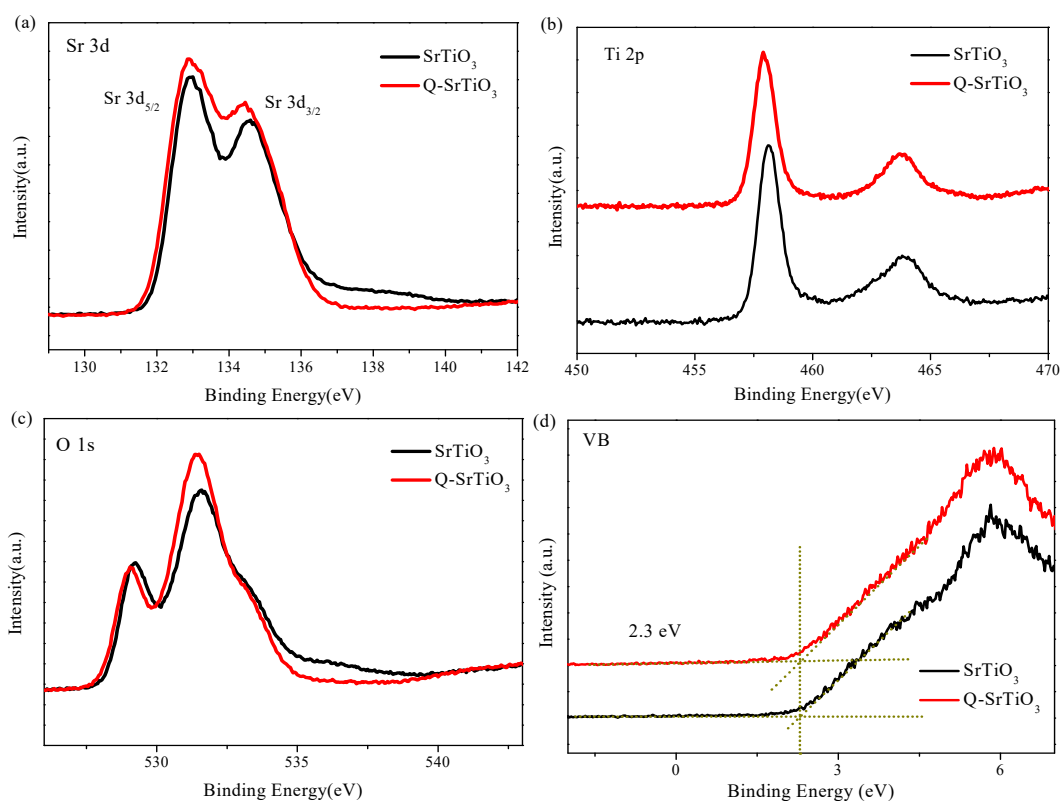


Figure 4. Sr 3d XPS spectra (a), Ti 2p XPS spectra (b), O1s Spectra (c), XPS valence band spectra of SrTiO₃ and Q-SrTiO₃ samples (d).

3.2. Photocatalytic Activity

The photodegradation of RhB in aqueous solution under visible-light irradiation was used to evaluate the photocatalytic activity of the Q-SrTiO₃, with SrTiO₃ as the control (Figure 5a). After adsorption-desorption equilibrium between the photocatalyst and the RhB solution was achieved in the absence of light, even a slight adsorption of RhB over the samples resulted in a slight decrease in the concentration of RhB. During the photodegradation process, SrTiO₃ showed no appreciable reduction in the RhB concentration in aqueous solution; however, Q-SrTiO₃ showed higher photocatalytic activity than SrTiO₃ in reducing the concentration of RhB in aqueous solution. After 370 min of visible-light irradiation in the presence of Q-SrTiO₃, RhB was decomposed by about 20%; in contrast, SrTiO₃ caused only 3% decomposition of the dye. The reaction constant (K_{app}) was calculated from the slope of the linear regression obtained from the plot of $-\ln(C/C_0)$ vs. time (Figure 5b). These results suggested that Q-SrTiO₃ shows better activity than SrTiO₃ for the photodegradation of RhB under visible light.

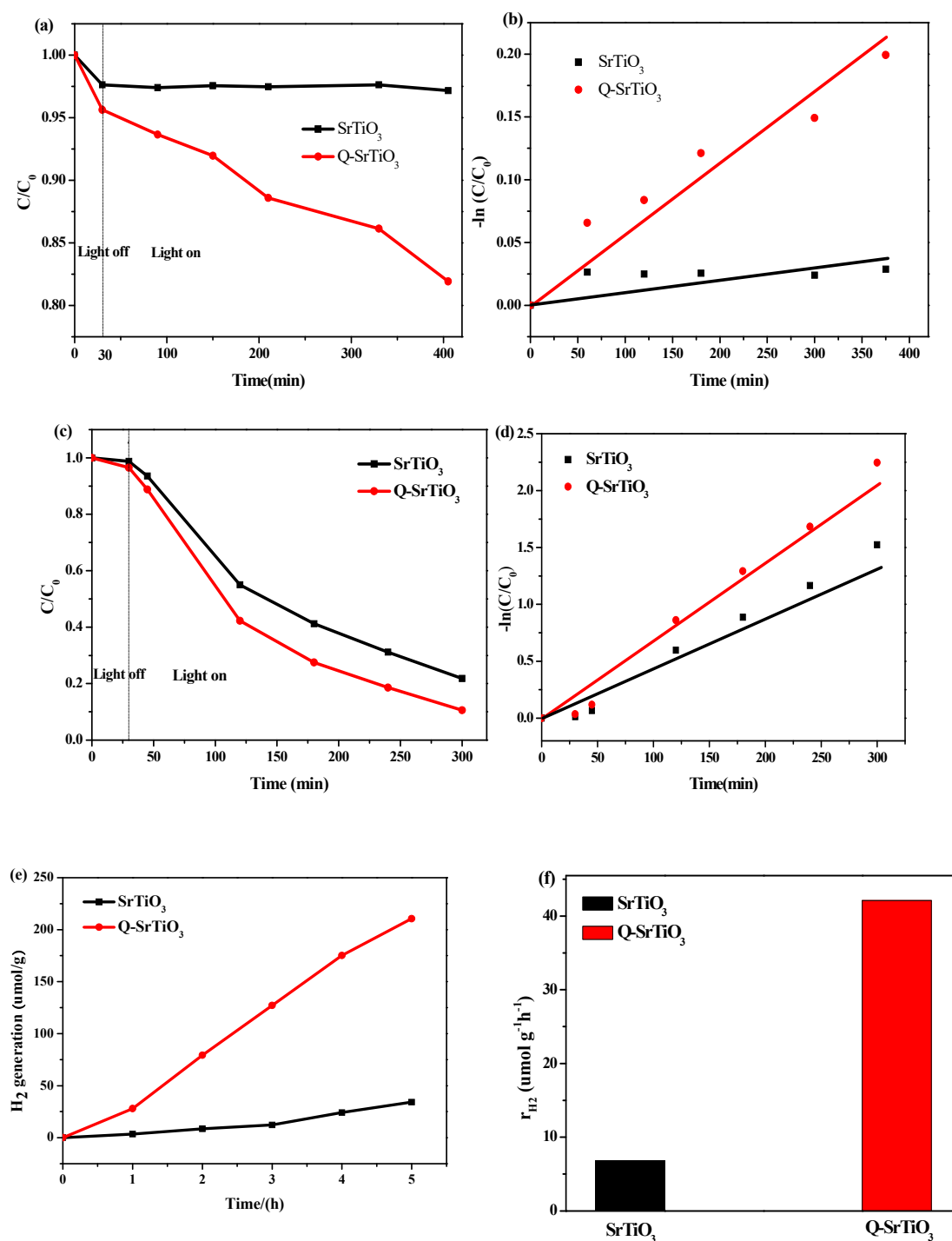


Figure 5. Photodecomposition of RhB aqueous solution with SrTiO₃ and Q-SrTiO₃ under visible light (a) and UV light (c). $-\ln(C/C_0)$ of the RhB concentration as a function of visible light (b) or UV light (d) irradiation time. Time-course of photocatalytic water splitting for H₂ generation in 100 mL 10% aqueous methanol solution under solar light (e). The rate of hydrogen generation for SrTiO₃ and Q-SrTiO₃ under solar light (f).

The UV-light photocatalytic activities of Q-SrTiO₃ were investigated by monitoring the decomposition of RhB in an aqueous solution, with SrTiO₃ as the control (Figure 5c,d). After 270 min of UV-light irradiation, the RhB dye was almost completely decomposed (~90%) by Q-SrTiO₃, (Figure 5c). The reaction constant (K_{app}) was shown in Figure 5d, this results also suggested that Q-SrTiO₃ shows better photocatalytic activity than SrTiO₃ for the photodegradation of RhB.

The photocatalytic activity of Q-SrTiO₃ for the photolysis of water to produce H₂ in 100 mL 10% aqueous methanol solution was also studied under solar irradiation, using SrTiO₃ as the control. Figure 5c,d present the time course of H₂ generation for SrTiO₃ and Q-SrTiO₃ under solar light irradiation. Q-SrTiO₃ steadily produced H₂ gas at the rate of 42.12 μmol g⁻¹ h⁻¹, which was almost 6.2 times higher than that observe with SrTiO₃ (6.83 μmol g⁻¹ h⁻¹). All these results demonstrated that Q-SrTiO₃ possesses higher photocatalytic activity than SrTiO₃.

4. Conclusions

In this paper, a facile and general method has been introduced to modify the surface environment of SrTiO₃ through an ethanol-quenching process. Q-SrTiO₃ showed higher photocatalytic activity than did SrTiO₃ for the degradation of RhB and the photolysis of water to produce H₂ under the irradiation by visible, UV or solar light. Results of spectroscopic characterization revealed that after rapid ethanol quenching, a high concentration of oxygen vacancies was introduced on the surface of the Q-SrTiO₃ lattice. Consequently, in order to maintain the regional charge balance in Q-SrTiO₃, the redundant Sr²⁺ is likely to substitute for Ti⁴⁺. Moreover, oxygen vacancies play an important role in enhancing the photocatalytic performance of Q-SrTiO₃ by not only inducing localized states into the band gap of Q-SrTiO₃, but also acting as photoinduced charge traps. Consequently, the light absorption ability is increased and the recombination rate of photogenerated electron-hole pairs is decreased, thus enhancing the photocatalytic activity of Q-SrTiO₃.

Author Contributions: Y.X.: performed photocatalysts synthesis, XRD, TEM, UV-visible absorption spectra analysis, photocatalytic activity tests and wrote the manuscript, S.C.: supervised rhodamine B and photocatalytic H₂ generation analysis in cooperation with Y.X., Y.W.: conceived the concept, designed the experiments, analyzed the data and revised the manuscript, Z.H.: performed EPR analysis, H.Z.: performed XPS analysis, W.X.: performed photocatalytic H₂ generation.

Funding: This research received no external funding.

Acknowledgments: This work is supported by the National Nature Science Foundation of China (No.21271048), Natural Science Foundation of China (11747074), Guangdong province science and technology plan project public welfare fund and ability construction project (2016A010103041, 2017A010103025), Doctoral Program of Lingnan Normal University (ZL1503), China Spark Program (2015GA780058).

Conflicts of Interest: The authors declare no conflict of interest.

References

1. Fujishima, A.; Honda, K. Electrochemical photolysis of water at a semiconductor electrode. *Nature* **1972**, *238*, 37–38. [[CrossRef](#)] [[PubMed](#)]
2. Chen, X.B.; Shen, S.H.; Guo, L.J.; Mao, S.S. Semiconductor-based photocatalytic hydrogen generation. *Chem. Rev.* **2010**, *110*, 6503–6570. [[CrossRef](#)] [[PubMed](#)]
3. Ran, J.R.; Zhang, J.; Yu, J.G.; Jaroniec, M.; Qiao, S.Z. Earth-abundant cocatalysts for semiconductor based photocatalytic water splitting. *Chem. Soc. Rev.* **2015**, *46*, 7787–7812. [[CrossRef](#)] [[PubMed](#)]
4. Wang, H.L.; Zhang, L.S.; Chen, Z.G.; Hu, J.Q.; Li, S.J.; Wang, Z.H.; Liu, J.S.; Wang, X.C. Semiconductor heterojunction photocatalysts: Design, construction, and photocatalytic performances. *Chem. Soc. Rev.* **2014**, *43*, 5234–5244. [[CrossRef](#)] [[PubMed](#)]
5. Dhakshinamoorthy, A.; Navalon, S.; Corma, A.; Garcia, H. Photocatalytic CO₂ reduction by TiO₂ and related titanium containing solids. *Energy Environ. Sci.* **2012**, *5*, 9217–9233. [[CrossRef](#)]
6. Pei, Z.X.; Weng, S.X.; Liu, P. Enhanced photocatalytic activity by bulk trapping and spatial separation of charge carriers: A case study of defect and facet mediated TiO₂. *Appl. Catal. B Environ.* **2016**, *180*, 463–470. [[CrossRef](#)]
7. Wu, Z.; Su, Y.F.; Yu, J.D.; Xiao, W.; Sun, L.; Lin, C.J. Enhanced photoelectrocatalytic hydrogen production activity of SrTiO₃-TiO₂ heteronanoparticle modified TiO₂ nanotube arrays. *Int. J. Hydrog. Energy* **2015**, *40*, 9704–9712. [[CrossRef](#)]
8. Wenderich, K.; Mul, G. Methods, mechanism, and applications of photodeposition in photocatalysis: A review. *Chem. Rev.* **2016**, *116*, 14587–14619. [[CrossRef](#)]

9. Grabowska, E. Selected perovskite oxides: Characterization, preparation and photocatalytic properties—A review. *Appl. Catal. B Environ.* **2016**, *186*, 97–126. [[CrossRef](#)]
10. Xie, T.H.; Sun, X.Y.; Lin, J. Enhanced photocatalytic degradation of RhB driven by visible light-induced MMCT of Ti(IV)–O–Fe(II) formed in Fe-doped SrTiO₃. *J. Phys. Chem. C* **2008**, *112*, 9753–9759. [[CrossRef](#)]
11. Ouyang, S.; Tong, H.; Umezawa, N.; Cao, J.; Li, P.; Bi, Y.; Zhang, Y.; Ye, J. Surface-alkalinization-induced enhancement of photocatalytic H₂ evolution over SrTiO₃-Based photocatalysts. *J. Am. Chem. Soc.* **2012**, *134*, 1974–1977. [[CrossRef](#)] [[PubMed](#)]
12. Liu, P.; Nisar, J.; Pathak, B.; Ahuja, R. Hybrid density functional study on SrTiO₃ for visible light photocatalysis. *Int. J. Hydrog. Energy* **2012**, *37*, 11611–11617. [[CrossRef](#)]
13. Yan, J.H.; Zhu, Y.R.; Tang, Y.G.; Zheng, S.Q. Nitrogen-doped SrTiO₃/TiO₂ composite photocatalysts for hydrogen production under visible light irradiation. *J. Alloy. Compd.* **2009**, *472*, 429–433. [[CrossRef](#)]
14. Luo, H.M.; Takata, T.; Lee, Y.; Zhao, J.F.; Domen, K.; Yan, Y.S. Photocatalytic Activity Enhanced for Titanium Dioxide by Co-doping with Bromine and Chlorine. *Chem. Mater.* **2004**, *16*, 846–849. [[CrossRef](#)]
15. Enterkin, J.A.; Setthapun, W.; Elam, J.W.; Christensen, S.T.; Rabuffetti, F.A.; Marks, L.D.; Stair, P.C.; Poepelmeier, K.R.; Marshall, C.L. Propane oxidation over Pt/SrTiO₃ nanocuboids. *ACS Catal.* **2011**, *1*, 629–635. [[CrossRef](#)]
16. Pan, X.W.; Wang, L.Q.; Ling, F.; Li, Y.H.; Han, D.X.; Pang, Q. A novel biomass assisted synthesis of Au-SrTiO₃ as a catalyst for hydrogen generation from formaldehyde aqueous solution at low temperature. *Int. J. Hydrog. Energy* **2015**, *40*, 1752–1759. [[CrossRef](#)]
17. Iwashina, K.; Kudo, A. Rh-doped SrTiO₃ photocatalyst electrode showing cathodic photocurrent for water splitting under visible-light irradiation. *J. Am. Chem. Soc.* **2011**, *133*, 13272–13275. [[CrossRef](#)] [[PubMed](#)]
18. Chambers, S.A.; Engelhard, M.H.; Shutthanandan, V.; Zhu, Z.; Droubay, T.C.; Qiao, L.; Sushko, P.V.; Feng, T.; Lee, H.D.; Gustafsson, T.; et al. Instability, intermixing and electronic structure at the epitaxial LaAlO₃/SrTiO₃(001) heterojunction. *Surf. Sci. Rep.* **2010**, *65*, 317–352. [[CrossRef](#)]
19. Tan, H.Q.; Zhao, Z.; Zhu, W.B.; Coker, E.N.; Li, B.S.; Zheng, M.; Yu, W.X.; Fan, H.Y.; Sun, Z.C. Oxygen vacancy enhanced photocatalytic activity of perovskite SrTiO₃. *ACS Appl. Mater. Interfaces* **2014**, *6*, 19184–19190. [[CrossRef](#)]
20. Wang, G.M.; Ling, Y.C.; Li, Y. Oxygen-deficient metal oxide nanostructures for photoelectrochemical water oxidation and other applications. *Nanoscale* **2012**, *4*, 6682–6691. [[CrossRef](#)]
21. Thompson, T.L.; Yates, J.T., Jr. TiO₂-based photocatalysis: surface defects, oxygen and charge transfer. *Top. Catal.* **2005**, *35*, 3–4. [[CrossRef](#)]
22. Chen, X.B.; Liu, L.; Yu, P.Y.; Mao, S.S. Increasing solar absorption for photocatalysis with black hydrogenated titanium dioxide nanocrystals. *Science* **2011**, *331*, 746–750. [[CrossRef](#)] [[PubMed](#)]
23. Yan, Y.; Han, M.Y.; Konkin, A.; Koppe, T.; Wang, D.; Andreu, T.; Chen, G.; Vetter, U.; Morante, J.R.; Schaaf, P. Slightly hydrogenated TiO₂ with enhanced photocatalytic performance. *J. Mater. Chem. A* **2014**, *2*, 12708–12716. [[CrossRef](#)]
24. Wang, G.M.; Wang, H.Y.; Ling, Y.C.; Tang, Y.C.; Yang, X.Y.; Fitzmorris, R.C.; Wang, C.C.; Zhang, J.Z.; Li, Y. Hydrogen-treated TiO₂ nanowire arrays for photoelectrochemical water splitting. *Nano Lett.* **2011**, *11*, 3026–3033. [[CrossRef](#)] [[PubMed](#)]
25. Wang, G.M.; Ling, Y.C.; Wang, H.Y.; Yang, X.Y.; Wang, C.C.; Zhang, J.Z.; Li, Y. Hydrogen-treated WO₃ nanoflakes show enhanced photostability. *Energy Environ. Sci.* **2012**, *5*, 6180–6187. [[CrossRef](#)]
26. Lu, X.H.; Wang, G.M.; Xie, S.L.; Shi, J.Y.; Li, W.; Tong, Y.X.; Li, Y. Efficient photocatalytic hydrogen evolution hydrogenated ZnO nanorod arrays. *Chem. Commun.* **2012**, *48*, 7717–7719. [[CrossRef](#)] [[PubMed](#)]
27. Zhao, W.L.; Zhao, W.; Zhu, G.L.; Lin, T.Q.; Xu, F.F.; Huang, F.Q. Black strontium titanate nanocrystals of enhanced solar absorption for photocatalysis. *CrystEngComm* **2015**, *17*, 7528–7534. [[CrossRef](#)]
28. Supphasrironjaroen, P.; Kongsuebchart, W.; Panpranot, J.; Mekasuwandumrong, O.; Satayaprasert, C.; Prasertthadam, P. Dependence of quenching process on the photocatalytic activity of solvothermal-derived TiO₂ with various crystallite sizes. *Ind. Eng. Chem. Res.* **2008**, *47*, 693–697. [[CrossRef](#)]
29. Dong, W.J.; Li, X.Y.; Yu, J.; Guo, W.C.; Li, B.J.; Tan, L.; Li, C.R.; Shi, J.J.; Wang, G. Porous SrTiO₃ spheres with enhanced photocatalytic performance. *Mater. Lett.* **2012**, *67*, 131–134. [[CrossRef](#)]
30. Feng, L.L.; Zou, X.X.; Zhao, J.; Zhou, L.J.; Wang, D.J.; Zhang, X.; Li, G.D. Nanoporous Sr-rich strontium titanate: a stable and superior photocatalyst for H₂ evolution. *Chem. Commun.* **2013**, *49*, 9788–9790. [[CrossRef](#)]

31. Tan, H.; Zhao, Z.; Niu, M.; Mao, C.; Cao, D.; Cheng, D.; Feng, P.; Sun, Z. A facile and versatile method for preparation of colored TiO₂ with enhanced solar-driven photocatalytic activity. *Nanoscale* **2014**, *6*, 10216–10223. [[CrossRef](#)] [[PubMed](#)]
32. Takata, T.; Domen, K. Defect engineering of photocatalysts by doping of aliovalent metal cations for efficient water splitting. *J. Phys. Chem. C* **2009**, *113*, 19386–19388. [[CrossRef](#)]
33. Hofman, W.; Hoffmann, R.W. Dopant influence on dielectric losses, leakage behaviour, and resistance degradation of SrTiO₃ thin films. *Thin Solid Film* **1997**, *305*, 66–73. [[CrossRef](#)]
34. Liu, B.S.; Cheng, K.; Nie, S.C.; Zhao, X.J.; Yu, H.G.; Yu, J.G.; Fujishima, A.; Nakata, K. Ice–water quenching induced Ti³⁺ Self-doped TiO₂ with surface lattice distortion and the increased photocatalytic activity. *J. Phys. Chem. C* **2017**, *121*, 19836–19848. [[CrossRef](#)]
35. Wagner, C.D. *Handbook of X-ray Photoelectron Spectroscopy*; Perkin-Elmer Corporation: Waltham, MA, USA, 1979.
36. Schaub, R.; Thostrup, P.; Lopez, N.; Lægsgaard, E.; Stensgaard, I.; Nørskov, J.K.; Besenbacher, F. Oxygen vacancies as active sites for water dissociation on rutile TiO₂(110). *Phys. Rev. Lett.* **2006**, *87*, 266104-1–266104-4. [[CrossRef](#)] [[PubMed](#)]



© 2019 by the authors. Licensee MDPI, Basel, Switzerland. This article is an open access article distributed under the terms and conditions of the Creative Commons Attribution (CC BY) license (<http://creativecommons.org/licenses/by/4.0/>).